

On the propagation times and energy losses of cosmic rays in the heliosphere

R. D. Strauss,¹ M. S. Potgieter,¹ A. Kopp,^{1,2} and I. Büsching^{1,3}

Received 12 May 2011; revised 30 August 2011; accepted 6 October 2011; published 17 December 2011.

[1] We present calculations of the propagation times and energy losses of cosmic rays as they are transported through the heliosphere. By calculating these quantities for a spatially 1D scenario, we benchmark our numerical model, which uses stochastic differential equations to solve the relevant transport equation, with known analytical solutions. The comparison is successful and serves as a vindication of the modeling approach. A spatially 3D version of the modulation model is subsequently used to calculate the propagation times and energy losses of galactic electrons and protons in different drift cycles. We find that the propagation times of electrons are longer than those of the protons at the same energy. Furthermore, the propagation times are longer in the drift cycle when the particles reach the Earth by drifting inward along the heliospheric current sheet. The calculated energy losses follow this same general trend. The energy losses suffered by the electrons are comparable to those of the protons, which is in contrast to the generally held perception that electrons experience little energy losses during their propagation through the heliosphere.

Citation: Strauss, R. D., M. S. Potgieter, A. Kopp, and I. Büsching (2011), On the propagation times and energy losses of cosmic rays in the heliosphere, *J. Geophys. Res.*, 116, A12105, doi:10.1029/2011JA016831.

1. Introduction

[2] After galactic cosmic rays (CRs) have entered the heliosphere, their intensities decrease as they propagate toward the Earth; a dynamical process referred to as CR modulation. In order to study the modulation of various species of CRs, the relevant transport equation (TPE) has to be solved. Because of the complexity of the TPE, and its associated transport coefficients, analytical solutions are only available for limited, mostly oversimplified cases and the implementation of numerical solutions (numerical modulation models) have become the norm. More recently, Monte Carlo type numerical models have become more widely implemented, solving a set of stochastic differential equations (SDEs) numerically to calculate differential CR intensities. The validity of these models in calculating CR fluxes have been discussed previously by, e.g., Yamada *et al.* [1998], Zhang [1999], and Pei *et al.* [2010]. SDE type models also allow for the calculation of CR propagation times (some authors refer to this as the residence or transit time; the time a CR takes to propagate from the heliopause to some observational point in the heliosphere) and energy losses, directly from the numerical scheme. The accuracy and

validity of these quantities, calculated using a SDE model, is tested in this work.

[3] The propagation times of CR have been a topic of study since Parker [1965] derived his original TPE. These analytical calculations were revisited by O'Gallagher [1975], who essentially found the propagation time to be energy dependent (more precisely, to be dependent on the diffusion coefficient, normally taken to be energy dependent), with longer propagation times for lower energy particles. This time-lag of CRs in responding to changing modulation conditions can explain the observed hysteresis effect in CR intensities as observed at Earth [e.g., O'Gallagher, 1975; Kane, 1981]. Recently, Florinski and Pogorelov [2009] demonstrated the advantage of SDE type models by calculating the propagation times of CRs in a more realistic (geometrically) 3D heliosphere, finding long propagation times for CRs in the turbulent heliosheath region. Interpreting the longer propagation time in this region as an indication of large amounts of energy being lost (via adiabatic cooling) by CRs is incorrect. The relation between the propagation times and energy losses is investigated further in this work.

[4] Similarly, the energy losses suffered by CRs propagating through the heliosphere have been studied extensively in the past, both theoretically [e.g., Parker, 1965, 1966; Jokipii and Parker, 1967; Webb and Gleeson, 1979, 1980] and observationally [e.g., Gleeson and Palmer, 1971; Urch and Gleeson, 1973], as well as through numerical modulation models [e.g., Goldstein *et al.*, 1970; Moraal and Potgieter, 1982; Zhang, 1999]. Zhang [1999] also illustrated the applicability of SDE type models in calculating this quantity. By examining these energy losses, insight can be

¹Centre for Space Research, North-West University, Potchefstroom, South Africa.

²Institut für Experimentelle und Angewandte Physik, Christian-Albrechts-Universität zu Kiel, Kiel, Germany.

³Institut für Theoretische Physik, Ruhr-Universität Bochum, Bochum, Germany.

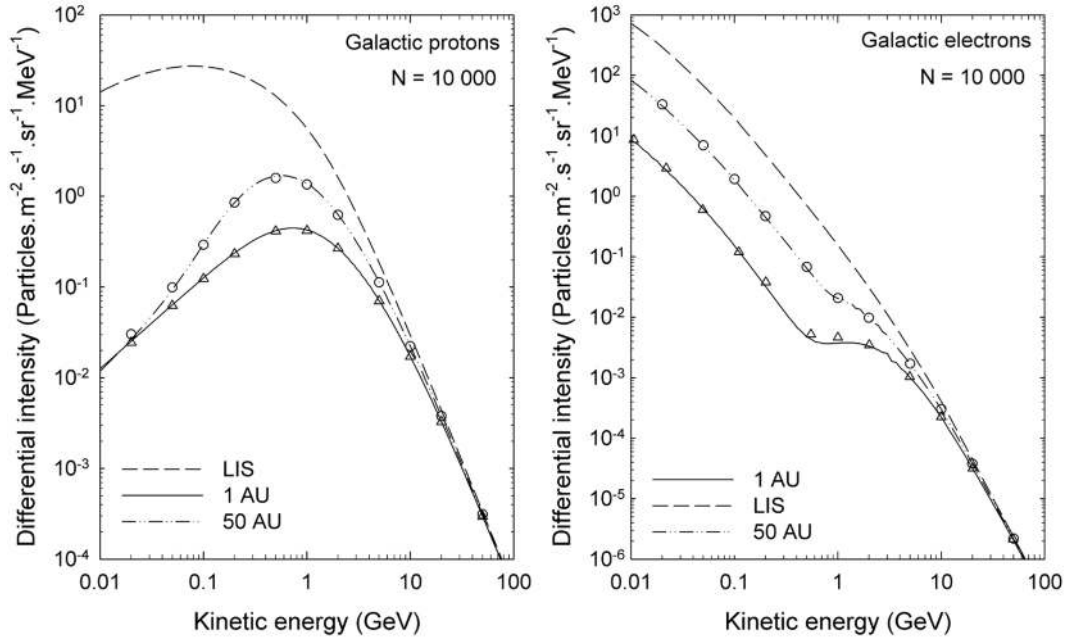


Figure 1. Energy spectra for galactic (left) protons and (right) electrons are shown as calculated by the SDE model (scatter points) and a finite difference numerical model (lines) at Earth (1 AU) and at 50 AU with the LIS specified at 100 AU. The dashed lines show the un-modulated local interstellar spectra at 100 AU. For these computations, $N = 10,000$ pseudo-particles were followed at each phase space position.

gained about, e.g., the effect of adiabatic cooling on the modeled and observed CR spectral shapes, as well as relating low energy CRs at Earth with their higher energy counterparts in the outer heliosphere.

[5] After the technique has been validated, the propagation times and energy losses of CR protons and electrons, in different drift cycles, are calculated using a 3D SDE model.

2. The Modulation Model

[6] The transport of CRs is described by the well known [Parker, 1965] transport equation (TPE). In terms of the omni-directional CR distribution function $f \equiv f(r, \theta, \phi, E, t)$, with r radial distance, θ polar angle, ϕ azimuthal angle and t time, the 1D version of the TPE is given by

$$\frac{\partial f}{\partial t} = \frac{1}{r^2} \frac{\partial}{\partial r} \left(r^2 \kappa \frac{\partial f}{\partial r} \right) - V_{sw} \frac{\partial f}{\partial r} + \frac{P}{3r^2} \frac{\partial}{\partial r} (r^2 V_{sw}) \frac{\partial f}{\partial P}. \quad (1)$$

[7] In these expressions, P is the particle rigidity, V_{sw} the solar wind speed and κ the effective radial diffusion coefficient (sometimes labeled as κ_{rr}). The differential intensity is related to f by $j = P^2 f$. For the spatially 1D case, equation (1) is essentially a diffusion-convection equation, but with the addition of energy losses/gains through the last term on the right hand side.

[8] For the spatially 3D scenario, the TPE has the form

$$\frac{\partial f}{\partial t} = -(\vec{V}_{sw} + \langle \vec{v}_d \rangle) \cdot \nabla f + \nabla \cdot (\mathbf{K}_s \cdot \nabla f) + \frac{P}{3} (\nabla \cdot \vec{V}_{sw}) \frac{\partial f}{\partial P} \quad (2)$$

with includes CR drifts through the pitch angle averaged guiding center drift velocity $\langle \vec{v}_d \rangle$ and diffusion described by the diffusion tensor \mathbf{K}_s .

[9] Solutions of the TPE have been used extensively in the past to model the transport and modulation of CRs for a variety of modulation conditions. The complexity of these models range from analytical solutions (only available for very limiting cases) to complex numerical models in higher dimensions. Most widely implemented in numerical modulation models are finite difference numerical schemes. These models, however, have several disadvantages, especially long computational time when solving the TPE in higher dimensions, and are notorious for their numerical instabilities. The focus has therefore shifted to implementing new algorithms and numerical methods, one of which is the use of stochastic differential equations (SDEs) to solve the TPE numerically. Several standard texts deal with this method, e.g., those by Gardiner [1983], Kloeden and Platen [1999], and Øksendal [2003], while heliospheric implementations of this method was discussed by, e.g., Fichtner et al. [1996], Yamada et al. [1998], Zhang [1999], and Pei et al. [2010]. The relevant SDEs, equivalent to equation (1), are

$$dr = \left[\frac{1}{r^2} \frac{\partial}{\partial r} (r^2 \kappa_{rr}) - V_{sw} \right] ds + \sqrt{2\kappa} \cdot dW_r \quad (3)$$

and

$$dP = \left[\frac{1}{3r^2} \frac{\partial}{\partial r} (r^2 V_{sw}) P \right] ds \quad (4)$$

for the radial and rigidity phase space coordinates respectively and ds indicating the infinitesimal (backwards) time

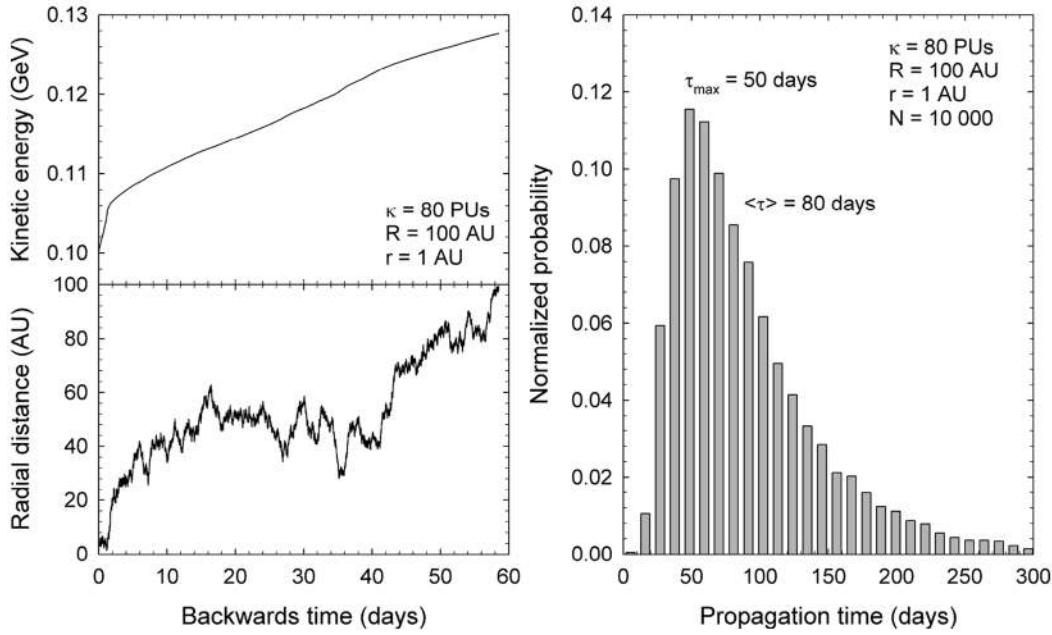


Figure 2. (left) An example of the evolution of a phase space density element (pseudo-particle), as described by the set of SDEs (for the spatially 1D case) in terms of (bottom) radial distance and (top) kinetic energy for galactic electrons. (right) The binned propagation time for $N = 10,000$ pseudo-particles.

increment. The rigidity SDE can also be rewritten in terms of kinetic energy E as

$$dE = \left[\frac{1}{3r^2} \frac{\partial}{\partial r} (r^2 V_{sw}) \Gamma E \right] ds, \quad (5)$$

with

$$\Gamma = \frac{E + 2E_0}{E + E_0}, \quad (6)$$

and E_0 the rest energy.

[10] For the 3D case, the SDEs, equivalent to equation (2), are

$$\begin{aligned} dr &= \left[\frac{1}{r^2} \frac{\partial}{\partial r} (r^2 \kappa_{rr}) + \frac{1}{r \sin \theta} \frac{\partial \kappa_{r\phi}}{\partial \phi} - V_{sw} - v_{dr} \right] ds \\ &\quad + \sqrt{2\kappa_{rr} - \frac{2\kappa_{r\phi}^2}{\kappa_{\phi\phi}}} dW_r + \frac{\sqrt{2}\kappa_{r\phi}}{\sqrt{\kappa_{\phi\phi}}} dW_\phi \\ d\theta &= \left[\frac{1}{r^2 \sin \theta} \frac{\partial}{\partial \theta} (\sin \theta \kappa_{\theta\theta}) - \frac{v_{d\theta}}{r} \right] ds + \frac{\sqrt{2\kappa_{\theta\theta}}}{r} dW_\theta \\ d\phi &= \left[\frac{1}{r^2 \sin^2 \theta} \frac{\partial \kappa_{\phi\phi}}{\partial \phi} + \frac{1}{r^2 \sin \theta} \frac{\partial}{\partial r} (r \kappa_{r\phi}) - \frac{v_{d\phi}}{r \sin \theta} \right] ds + \frac{\sqrt{2\kappa_{\phi\phi}}}{r \sin \theta} dW_\phi \\ dE &= \left[\frac{1}{3r^2} \frac{\partial}{\partial r} (r^2 V_{sw}) \Gamma E \right] ds \end{aligned} \quad (7)$$

for the different phase space components. For a derivation of these equations, see, e.g., *Strauss et al.* [2011].

[11] To solve the SDEs, the so-called time backwards approach is adopted, solving the set of SDEs numerically by using the Euler-Maruyama scheme [*Maruyama*, 1955]. In this approach, an initial phase space point (r^0, E^0) is specified (which is also the point at which j will be obtained; the so-called observational point) at the backwards time $s = 0$.

The evolution of this phase space point, for $s > 0$, is then calculated iteratively according to equations (3) and (5), i.e., $r^{n+1} = r^n + dr$ and $E^{n+1} = E^n + dE$ until a boundary is reached at (r^e, E^e) at time s^e . For galactic CRs, this is assumed to be the HP, where their intensities are prescribed by a CR species specific LIS. For electrons the LIS of *Langner et al.* [2001] is used, while for protons we use the LIS of *Moskalenko et al.* [2002]. For further details of the numerical implementation used in the modulation model, see *Strauss et al.* [2011]. The superscript “e” refers to the exit position (in the time backwards formulation; in the normal time forwards scenario, this can be called the entry position) of this phase space point (pseudo-particle) being followed. Calculating these trajectories for a large number of pseudo-particles, we then obtained an average value of $j(r^0, E^0)$.

[12] Figure 1 shows, as an example, solutions of the 1D TPE for the modulation of galactic protons (Figure 1, left) and electrons (Figure 1, right) at Earth and at 50 AU, with respect to the local interstellar spectrum (LIS), as the scatter points. The lines are numerical solutions of the same equation using the Du Fort-Frankel numerical scheme. For these solutions, the outer boundary (heliopause, HP) is assumed to be located at $R = 100$ AU for illustrative purposes, $V_{sw} = 400$ km.s⁻¹ and a mean free path of the form $\lambda = 0.1$ AU $\cdot (P/1$ GV) is used for protons and electrons when $P > 1$ GV. Below 1 GV, $\lambda = 0.1$ AU was used for electrons. Note that $\kappa = v\lambda/3$ with v the particle speed. The obtained results are consistent with similar benchmark solutions given by, e.g., *Yamada et al.* [1998] and *Pei et al.* [2010], illustrating the validity and usefulness of the SDE approach in solving the TPE.

[13] Figure 2 (left) shows a realization of a single phase space point starting at $(r^0, E^0) = (1$ AU, 0.1 GeV) and ending at $(r^e, E^e) \approx (100$ AU, 0.13 GeV). This is done for galactic electrons with a constant diffusion coefficient

of $\kappa = 80$ PUs, where PUs refers to program units ($1 \text{ PU} = 6 \times 10^{20} \text{ cm}^2 \cdot \text{s}^{-1}$), introduced for shorter notation.

[14] The SDE approach allows for the calculation of the propagation time of CRs directly from the numerical method. For the realization of a single pseudo-particle, labeled by the index i , the propagation time is simply the time it takes for the pseudo-particle to be transported, for the 1D case, from r^0 to r^e , calculated as

$$\tau_i = |s_i^e - s_i^0|. \quad (8)$$

[15] Calculating τ for a single pseudo-particle is however statistically insignificant. Therefore, τ_i is calculated for a large number of these particles (usually $N > 3000$) and binned in a normalized histogram. The expectation value is calculated as the weighted average of τ_i , as

$$\langle \tau \rangle = \sum_{l=1}^M \tau_l \rho_l, \quad (9)$$

where M refers to the number of bins in the distribution and ρ_l is the probability of finding τ_i in the time bin τ_l ,

$$\rho_l = \frac{N_l}{N}, \quad (10)$$

with N_l the number of particles ending up in the l -th bin and the normalization condition

$$\sum_{l=1}^M \rho_l = 1 \quad (11)$$

automatically satisfied.

[16] Figure 2 (right) shows the normalized binned propagation time of $N = 10,000$ pseudo particles (in this case galactic electrons). Two timescales are indicated on the figure, namely: τ_{\max} which is the most probable propagation time and $\langle \tau \rangle$ which is the average propagation time (i.e., the expectation value thereof). Because of the long tail in the distribution of τ , we generally find $\langle \tau \rangle > \tau_{\max}$. For the rest of this paper we consider only the behavior of $\langle \tau \rangle$.

[17] Since we use the time backwards approach to solve the relevant SDEs, this normalization to unity is characteristic of the method of solution; in the normal time forward case this corresponds to all particles entering the heliosphere eventually reaching a point r^0 in the inner heliosphere, after some time $\tau > 0$. In later sections this normalization of the propagation time is discussed further.

[18] Similar to $\langle \tau \rangle$, the SDE approach also allows for the direct calculation of the energy loss by a CR during its propagation through the heliosphere. Again the expectation value of the exit energy $\langle E^e \rangle$, can be calculated (in the time forward scenario, E^e would refer to the energy of a CR directly before entering the heliosphere). The average amount of energy loss during the propagation process is then

$$\langle \Delta E \rangle = \langle E^e \rangle - E^0. \quad (12)$$

[19] For this work, the focus is on galactic electrons and protons. CR electrons are highly relativistic for all energies considered, so that $E \gg E_0$ and $\Gamma \rightarrow 1$. Galactic protons of $E > 100$ MeV are however somewhere in between

a totally relativistic and totally non-relativistic case. For fully non-relativistic CRs, $E \ll E_0$ and $\Gamma \rightarrow 2$.

3. Case 1: A Diffusion Dominated Scenario

3.1. Propagation Times: Analytical Approximations

[20] In his seminal paper, *Parker* [1965] introduced the probability wave approach to study the propagation times of CRs. Instead of computing the differential intensity of the CRs, this approach calculates the probability $w(r, t)$ of finding a particle at a position r at a time t . Choosing a constant (energy and spatially independent) diffusion coefficient in 1D, the processes that influence CR transport are convection and diffusion. The evolution of $w(r, t)$ thus satisfies the convection-diffusion Fokker-Planck equation

$$\frac{\partial w(r, t)}{\partial t} = \frac{1}{r^2} \frac{\partial}{\partial r} \left(r^2 \kappa \frac{\partial w(r, t)}{\partial r} \right) - V_{sw} \frac{\partial w(r, t)}{\partial r}, \quad (13)$$

with the first term on the left hand side referring to the inward diffusion of galactic cosmic rays and the second term the outward convection by the solar wind and embedded magnetic field. As a first application of this model, we assume the system to be diffusion dominated and neglect convection by setting the solar wind speed to $V_{sw} = 0$. For this scenario, equation (13) can be solved analytically quite easily. As an initial condition, an empty heliosphere is assumed and the CR particles are introduced at a radial position of $r = R - h$ at $t = 0$ where R is the radius of the outer boundary (HP) and h the penetration length of a galactic CR, i.e., the distance it penetrates the heliosphere before being scattered for the first time. With these assumptions, using a free-escape outer boundary (CRs are free to leave the heliosphere) and a reflecting inner boundary at $r = 0$, *Parker* [1965] obtained

$$w(r, t) \approx \frac{h}{2R^3 r} \sum_{n=1}^{\infty} (-1)^{n-1} n \sin\left(\frac{n\pi r}{R}\right) \exp\left(-\frac{n^2 \pi^2 \kappa t}{R^2}\right), \quad (14)$$

valid for $h \ll R$. As $w(r, t)$ is a probability, it can be re-normalized to unity because of the linearity of equation (13). Figure 3 (left) shows $w(r, t)$ as a function of normalized distance. The numbers in brackets label the curves according to the dimensionless parameters $(RV_{sw}/\kappa, \kappa t/R^2)$. Assuming κ and R to be constant, the curves can be interpreted as showing the temporal evolution of $w(r, t)$. Starting from an initial delta function, the probability wave diffuses spatially, getting reflected at the inner boundary, and finally being absorbed at the outer boundary, i.e., when $t \rightarrow \infty$, $w(r, t) \rightarrow 0$. Figure 3 (right) shows the temporal evolution of $w(r, t)$ at a constant radial position of $r/R = 0.01$ (i.e., 1 AU for this choice of R). Starting from zero at $t = 0$, the probability of finding a particle at this position increases sharply to a maximum (the most probable propagation time), where after it decreases again to zero, following an almost Poisson like distribution.

[21] The expectation value ($\langle \tau \rangle$) of the propagation time is calculated, for a particular spatial point $r_a < R$, as

$$\langle \tau \rangle = \frac{\int_{t=0}^{\infty} w(r_a, t) t dt}{\int_{t=0}^{\infty} w(r_a, t) dt}. \quad (15)$$

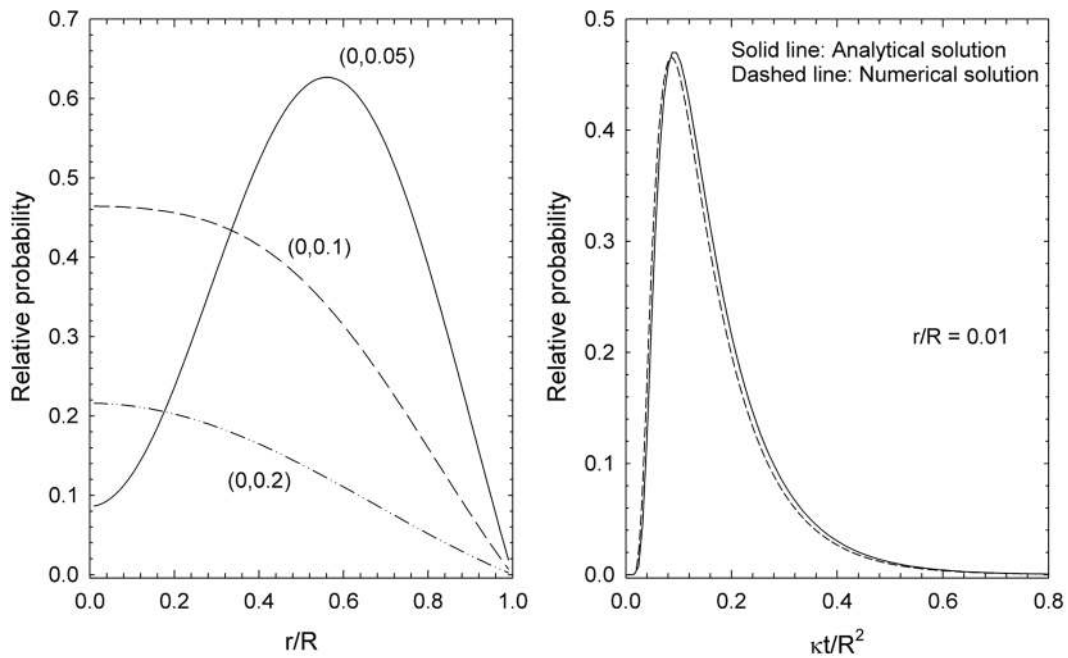


Figure 3. (left) Plot of $w(r, t)$ as a function of radial distance. The curves are labeled by values for $(RV_{sw}/\kappa, \kappa t/R^2)$ with $V_{sw} = 0$ when convection is neglected. (right) The temporal evolution of $w(r, t)$ at a fixed spatial point. The solid line is the analytical solution of equation (13), while the dashed line is a numerical solution of the same equation, discussed in section 4.1.

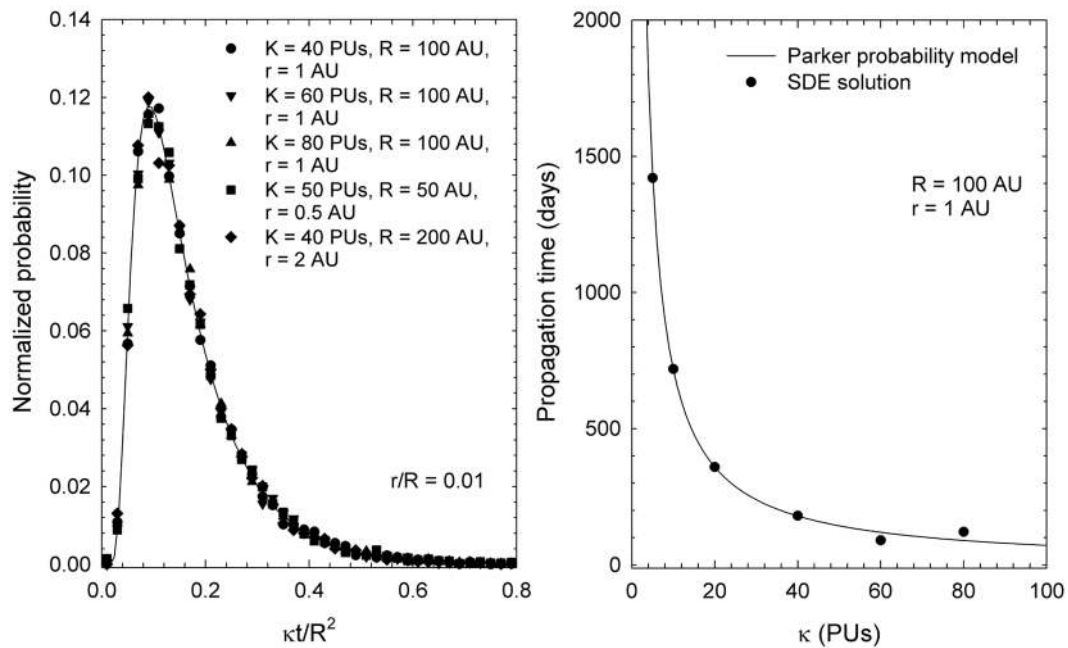


Figure 4. (left) The binned propagation times as calculated with the SDE model for different transport parameters (scatter points) at a radial position of $r/R = 0.01$; the solid line shows the re-normalized probability, initially shown in Figure 3 (right). (right) Plot of $\langle \tau \rangle$, as calculated with equation (16), with $R = 100$ AU, as the solid line; the scatter points show $\langle \tau \rangle$ as a function of κ as calculated with the SDE model.

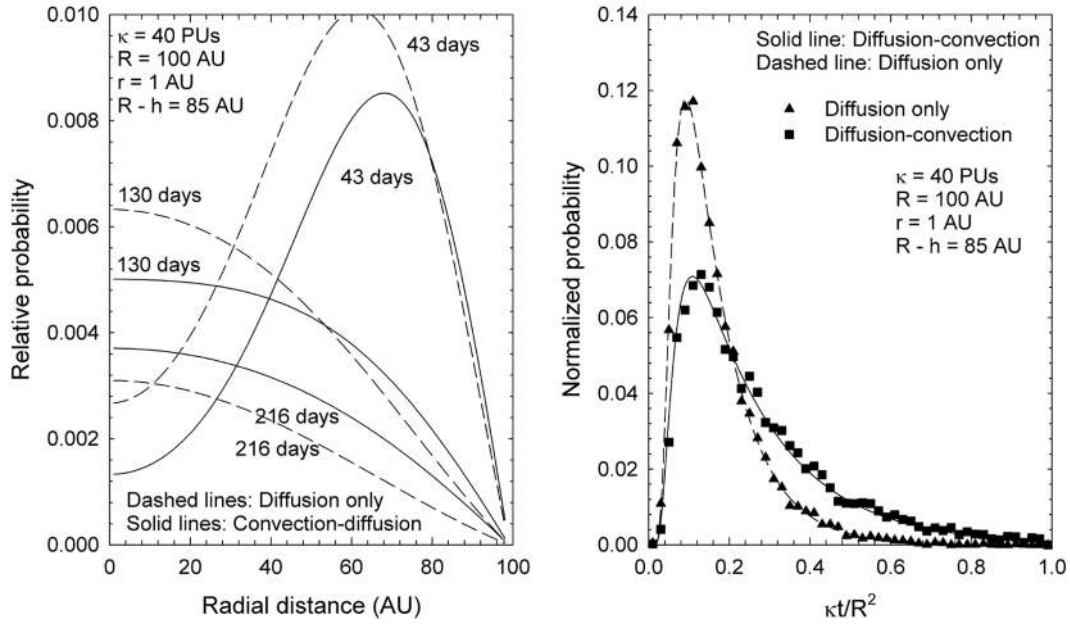


Figure 5. (left) The numerically calculated $w(r, t)$ as a function of radial distance at different times, including convection (solid lines) and neglecting convection (dashed lines) in the model for the parameters as indicated. (right) Plot of $w(r, t)$ as a function of time, for the different cases, at $r = 1$ AU. The scatter points show the corresponding solutions from the SDE model.

[22] Again this equation can be solved analytically to give

$$\langle \tau_d \rangle = \frac{R^2}{\pi^2 \kappa} \sum_{n=1}^{\infty} \frac{1}{n^2} \rightarrow \frac{R^2}{6\kappa}, \quad (16)$$

where the subscript “d” indicates that this is the average propagation time when only diffusion is considered. *O’Gallagher* [1975] derived the same expression for $\langle \tau_d \rangle$ and refers to this as the diffusion timescale. Note that $\langle \tau_d \rangle$ is inversely proportional to κ and that $\langle \tau_d \rangle \rightarrow \infty$ when $\kappa \rightarrow 0$, while $\langle \tau_d \rangle \rightarrow 0$ when $\kappa \rightarrow \infty$.

3.2. Propagation Times: SDE Approach

[23] The SDE solutions shown and discussed in this section neglect solar wind convection consistent with the analytical approximations discussed in the previous section. Figure 4 (left) shows the binned propagation times from the SDE model as scatter points. This is similar to Figure 2 (right), but with the time expressed as $\kappa t/R^2$ using different combinations of κ and R . All solutions are shown at a constant (normalized) radial position of $r_a = r/R = 0.01$. The dashed line shows the analytical solution, given by equation (14), with the probability $w(r, t)$ re-normalized so that

$$\int_{t=0}^{\infty} w(r_a, t) dt = 1, \quad (17)$$

in line with the results from the SDE model where all CRs entering the heliosphere will penetrate up to r_a . The solutions of the SDE model compare very well with the analytical approximation, confirming the reliability of the results generated with the SDE model. In order to test the

validity of equation (16), Figure 4 (right) shows $\langle \tau \rangle$, as calculated with equation (16), as the solid line, while the scatter points show the results from the SDE model for the same scenario. Again, excellent agreement between the two methods are obtained, which we consider as the validation of the SDE approach in calculating $\langle \tau \rangle$.

4. Case II: A Diffusion-Convection Scenario

4.1. Propagation Times: Analytical and Numerical Approximations

[24] The solutions of the previous sections neglected the outward convection by the solar wind, which is now included. As shown by *Parker* [1965] and *O’Gallagher* [1975], analytical solutions of equation (13) are possible only for very limited cases. Therefore we solve the probability wave equation numerically, where κ is again assumed to be constant and the equation is solved by a finite differences scheme. Figure 3 (right) already showed the numerical solution as the dashed line, using $R = 100$ AU and $h = 15$ AU, compared to the analytical solution of *Parker* [1965] as the solid line.

[25] In Figure 5 (left), $w(r, t)$, as calculated numerically, is shown as a function of radial distance at different times. Two solutions are shown: including convection (solid lines) and neglecting convection in the model (dashed lines). With the inclusion of outward convection, it is clear that the CRs find it more difficult to reach the inner heliosphere. Figure 5 (right) shows $w(r, t)$ as a function of time at $r = 1$ AU (Earth) for the same two cases shown in Figure 5 (left). What is notable from the solutions is that τ_{\max} is approximately equal for the different cases. However, the calculated distribution including convection is much wider than the case

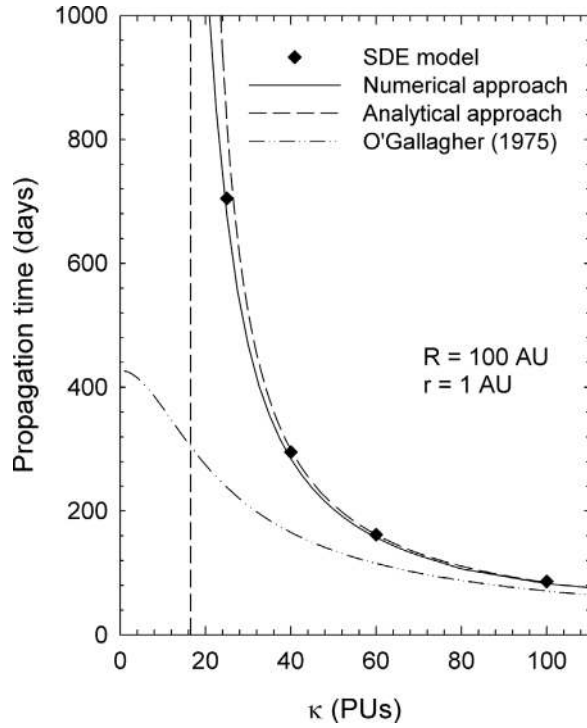


Figure 6. The propagation time as a function of κ for the convection-diffusion model. Scatter points show results of the SDE model, the solid line of the numerical probability wave approach, the dashed line the derived analytical solution given by equation (22) and the dashed-dotted line the analytical solution of *O'Gallagher* [1975].

including only diffusion, so that $\langle \tau \rangle$ is clearly longer for this case. This is expected, as inward diffusing CR scattering centers are continuously convected outwards, making it harder for CRs to reach the inner heliosphere, and subsequently taking longer to do so.

[26] Next, assume a CR scattering center originally located at $r = R$. Equation (16) gives the average propagation time of the scattering center to reach $r = 0$ when only diffusion is considered. The average velocity at which the scattering centers diffuse inward, covering a distance R , is then

$$\langle \vec{v}_d \rangle = -\frac{6\kappa}{R} \mathbf{e}_r. \quad (18)$$

[27] If outward convection with a speed of V_{sw} is also considered, the net transport velocity is then

$$\langle \vec{v}_{cd} \rangle = V_{sw} \mathbf{e}_r - \frac{6\kappa}{r} \mathbf{e}_r. \quad (19)$$

[28] To be displaced by $-\mathbf{R}\mathbf{e}_r$, the scattering center will thus take a time

$$\langle \tau_{cd} \rangle = \frac{R^2}{6\kappa - V_{sw}R}. \quad (20)$$

[29] Introducing the characteristic convection time as

$$\langle \tau_c \rangle = \frac{R}{V_{sw}}, \quad (21)$$

i.e., the time it takes for a scattering center to be transported from $r = 0$ to $r = R$ without undergoing diffusion, equation (20) can be rewritten more compactly as

$$\langle \tau_{cd} \rangle = \left[\frac{1}{\langle \tau_d \rangle} - \frac{1}{\langle \tau_c \rangle} \right]^{-1}, \quad (22)$$

giving the approximate propagation time in the convection-diffusion model. Note that when $\langle \tau_c \rangle \rightarrow \infty$, $\langle \tau_{cd} \rangle \rightarrow \langle \tau_d \rangle$ and when $\langle \tau_c \rangle \rightarrow \langle \tau_d \rangle$, $\langle \tau_{cd} \rangle \rightarrow \infty$, i.e., when the convective and diffusive processes are in equilibrium, a CR will remain at a radial position $0 < r < R$ indefinitely. When $\langle \tau_c \rangle < \langle \tau_d \rangle$ (equivalently, $\langle v_d \rangle < \langle v_c \rangle$) the CR will be convected to $r > R$ and cannot spend any time in the heliosphere. From equation (22), this situation occurs when $\langle \tau_{cd} \rangle < 0$.

4.2. Propagation Times: SDE Approach

[30] In Figure 5 (right), the resulting propagation times calculated with the SDE model are compared to the results from the probability wave model. These calculations use $\kappa = 40$ PUs and $V_{sw} = 400 \text{ km.s}^{-1}$ with the propagation times shown for the cases when solar wind convection is included or neglected. Again, very good agreement is obtained between the different approaches.

[31] In Figure 6, $\langle \tau \rangle$ is shown as a function of κ , with the effects of convection included. The scatter points show results from the SDE model and the solid lines $\langle \tau \rangle$ as calculated from the numerical wave probability approach. The dashed line shows $\langle \tau_{cd} \rangle$, calculated from equation (22), while the dash-dotted line show $\langle \tau \rangle$ as calculated by *O'Gallagher* [1975]. The vertical dashed line shows the value of κ where $\langle \tau_{cd} \rangle \rightarrow \infty$. For larger values of κ the analytical approximation of the previous section seems reasonable, whereas small deviations occur at lower values of κ . The analytical solution of *O'Gallagher* [1975], however, deviates completely with the results from the SDE model with $\langle \tau_{cd} \rangle \rightarrow \langle \tau_c \rangle$ as $\kappa \rightarrow 0$; a non-physical situation for galactic CRs in the heliosphere.

4.3. Energy Losses

[32] In his original derivation of the TPE, *Parker* [1965] derived the CR energy loss term as

$$\mathfrak{I} = -\frac{\partial}{\partial E} \left(\frac{\partial E}{\partial t} f \right), \quad (23)$$

where

$$\frac{\partial E}{\partial t} = -\frac{1}{3} (\nabla \cdot \vec{V}_{sw}) \Gamma E = -\frac{1}{3r^2} \frac{\partial}{\partial r} (r^2 V_{sw}) \Gamma E \quad (24)$$

is the rate at which CRs are adiabatically cooled in the expanding solar wind and f the CR distribution function. As pointed out by, e.g., *Fisk* [1979], $\nabla \cdot \vec{V}_{sw}$ is the rate at which a solar wind volume element expands as it moves radially outwards with a speed of V_{sw} . Equation (23) is derived by assuming that adiabatic cooling is the only mechanism

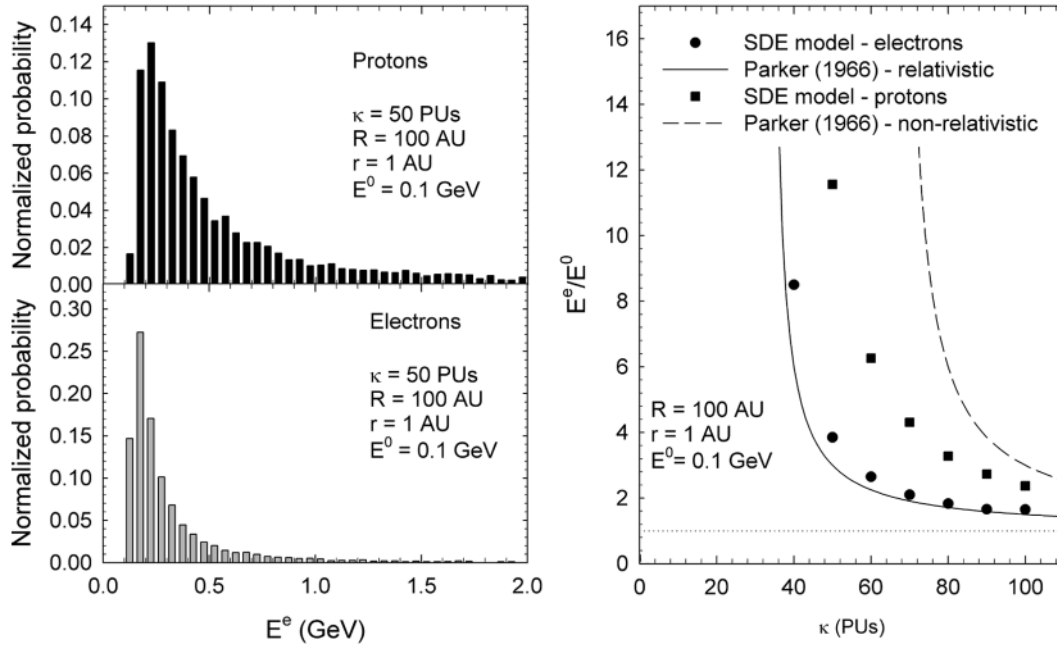


Figure 7. (left) The normalized probability of E^e from the SDE model for 10000 pseudo-particles for (top left) protons and (bottom left) electrons. (right) The scatter point shows $\langle E^e/E^0 \rangle$ as a function of κ , as calculated from the SDE model. The solid line is the analytical approximation of equation (32) for relativistic CRs, the dashed line for non-relativistic CRs and the horizontal dotted line shows the limiting case of $\langle E^e/E^0 \rangle = 1$.

responsible for CR energy losses. In terms of momentum, the average deceleration rate is

$$\langle \dot{p}' \rangle = \left\langle \frac{dp'}{dt} \right\rangle' = -\frac{p'}{3r^2} \frac{\partial}{\partial r} (r^2 V_{sw}). \quad (25)$$

[33] As however discussed by, e.g., *Webb and Gleeson* [1979], this rate is only valid if the CRs are described with respect to a frame co-moving with the solar wind at a speed of V_{sw} . In a coordinate system fixed on the Sun (heliocentric coordinates), the momentum loss rate has the form

$$\langle \dot{p} \rangle = -\frac{p}{3} \vec{V}_{sw} \cdot \vec{g}_r \quad (26)$$

[e.g., *Webb and Gleeson*, 1979], where \vec{g}_r is the radial CR differential intensity gradient. Although these momentum loss rates differ from each other, the resulting TPE remains unchanged, largely because of the Compton-Getting factor [e.g., *Gleeson and Axford*, 1968; *Forman*, 1970; *Webb and Gleeson*, 1980].

[34] To calculate the total energy lost by CRs propagating through the heliosphere, the analytical approach of *Parker* [1965, 1966] and *Jokipii and Parker* [1970] is used, where the differential intensity, $j(r, E, t)$ in terms of kinetic energy, is obtained by deconvolving the equation

$$w(r, t) = \int_0^\infty j(r, E, t) dE. \quad (27)$$

[35] This model introduces a constant stream of particles at $r = R$ with an energy of E^e , and calculates the average energy $\langle E^0 \rangle$ of the particles reaching $r = 0$, as

$$\langle E^0 \rangle = \frac{\int_0^{E^e} E j(0, E, t) dE}{\int_0^{E^e} j(0, E, t) dE} \quad (28)$$

with

$$\frac{E^e}{\langle E^0 \rangle} = \left\langle \frac{E^e}{E^0} \right\rangle \quad (29)$$

the average fractional energy loss. In the limit of

$$\frac{RV_{sw}}{\kappa} \ll 1, \quad (30)$$

equation (28) was solved by *Parker* [1966] to give

$$\langle E^0 \rangle - E^e = -\frac{\Gamma}{3} E^e \frac{RV_{sw}}{\kappa}, \quad (31)$$

or in terms of the fractional energy loss as

$$\left\langle \frac{E^e}{E^0} \right\rangle = \left(1 - \frac{\Gamma}{3} \frac{RV_{sw}}{\kappa} \right)^{-1}, \quad (32)$$

satisfying the limiting case of $\langle E^e/E^0 \rangle \rightarrow 1$ when $\kappa \rightarrow \infty$, i.e., for very large values of κ the CRs will loose no energy.

[36] In the time backwards SDE approach used here, CRs are introduced at $r = 1$ AU with an energy of E^0 . They then propagate toward the outer heliosphere, continually gaining energy adiabatically, and reach the HP with an energy of $E^e > E^0$. In this section, the SDE model incorporates convection and uses a value of $E^0 = 0.1$ GeV. Figure 7 (left)

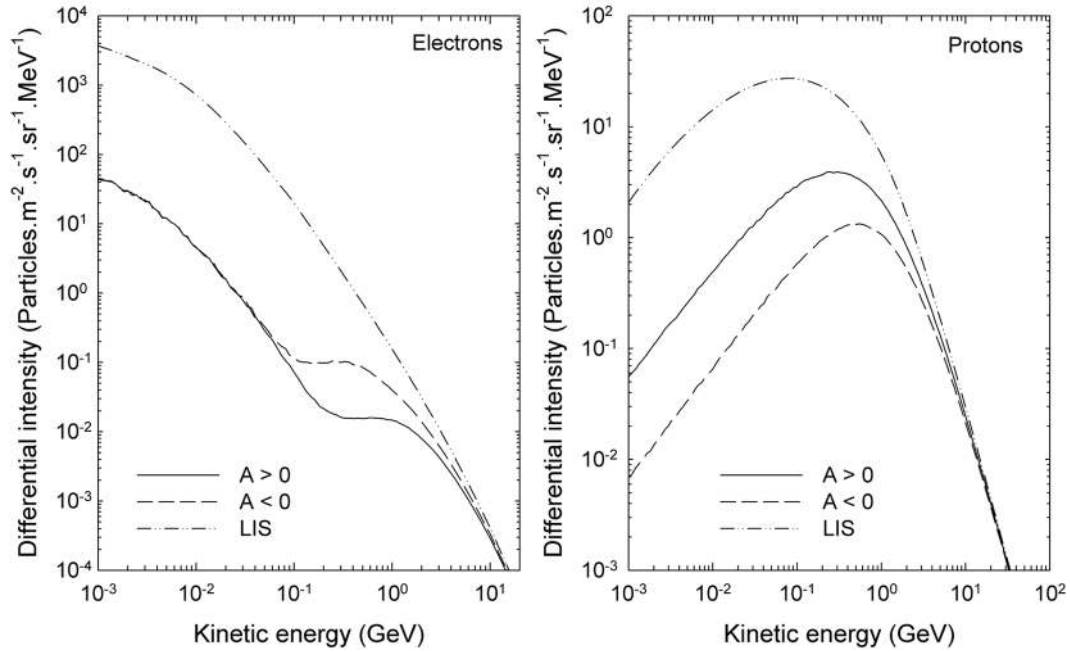


Figure 8. Modeled energy spectra at Earth, with respect to the LIS at $R = 120$ AU, for galactic (left) electrons and (right) protons for both HMF polarity cycles, indicated by $A < 0$ and $A > 0$, using the 3D SDE modulation model.

shows binned values of E^e for 10000 individual pseudo-particles; Figure 7 (top left) for protons and Figure 7 (bottom left) for electrons. As expected, $E^e > E_0$, with no apparent upper limit to the fractional energy loss. The expectation value $\langle E^e/E^0 \rangle$ is calculated, and shown as a function of κ in Figure 7 (right) as scatter points. As expected, the fractional energy loss increases with decreasing values of κ . The solid line shows the analytical approximation of equation (32), for relativistic CRs ($\Gamma = 1$), the dashed line the same approximation but for non-relativistic CRs ($\Gamma = 2$), while the horizontal dotted line shows the limiting case of $\langle E^e/E^0 \rangle = 1$. The SDE electron solutions and the $\Gamma = 1$ approximation agrees quite well. For protons, the fractional energy loss is expected to be somewhere in between the $\Gamma = 1$ and $\Gamma = 2$ approximations, and this is indeed what the SDE model gives. These good comparisons between the results indicate the validity of the SDE approach in calculating the energy losses suffered by CRs.

5. The 3D SDE Model: Galactic Electrons and Protons

[37] Using the 3D SDE modulation model, energy spectra at Earth are shown in Figure 8 for galactic electrons (Figure 8, left) and protons (Figure 8, right). Using a *Parker* [1958] heliospheric magnetic field (HMF), solutions are shown for both the $A < 0$ (Figure 8, left) and $A > 0$ (Figure 8, right) HMF polarity cycles, illustrating the effect of gradient and curvature drifts in the model. The drift velocity is incorporated into the model as discussed by *Strauss et al.* [2011], which includes curvature, gradient and neutral sheet drifts. For the latter, a flat current sheet drift model is adopted. For the diffusion

coefficient parallel to the mean HMF, the following form was used

$$\kappa_{\parallel} = \kappa_0 \frac{P}{P_0} \left(1 + \frac{r}{r_0} \right) \quad (33)$$

with $r_0 = 1$ AU, $P_0 = 1$ GV and $\kappa_0 = 25$ PUs for protons and electrons above 1 GV. Below 1 GV, an energy independent κ_{\parallel} was used for electrons, with $P/P_0 \equiv 1$. Furthermore, isotropic perpendicular diffusion with $\kappa_{\perp r} = \kappa_{\perp \theta} = 0.02\kappa_{\parallel}$ [*Giacalone and Jokipii*, 1999] was assumed. The diffusion tensor is thus qualitatively similar to the one used by *Potgieter and Moraal* [1985].

[38] Analytical approximations of CR energy losses in the spatially 3D scenario are impossible and must thus be studied with numerical modulation models. The traditional way of computing this is shown for illustrative purposes in Figure 9: At the HP, a near Gaussian input spectrum is specified. This input spectrum is then modulated, with the resulting distribution at Earth investigated. In Figure 9, nine of these peaks are introduced at the HP for electrons (Figure 9, left) and protons (Figure 9, right). The corresponding modulated distributions at Earth are also shown (with the numbers labeling the individual pairs of solutions), with the intensities normalized at the HP to LIS levels. Examining how these initial peaks modulate, gives some indication of the energy losses suffered by the CRs. Normally, only the shift in energy of the peak's maximum intensity is taken as the energy loss, i.e., for protons, peak 7 is introduced at the HP with $E \approx 1$ GeV, while it ends up at Earth at $E \approx 0.5$ GeV, giving an energy loss of $\Delta E \approx 500$ MeV. This however does not give the entire picture as the modulated intensities at Earth, as

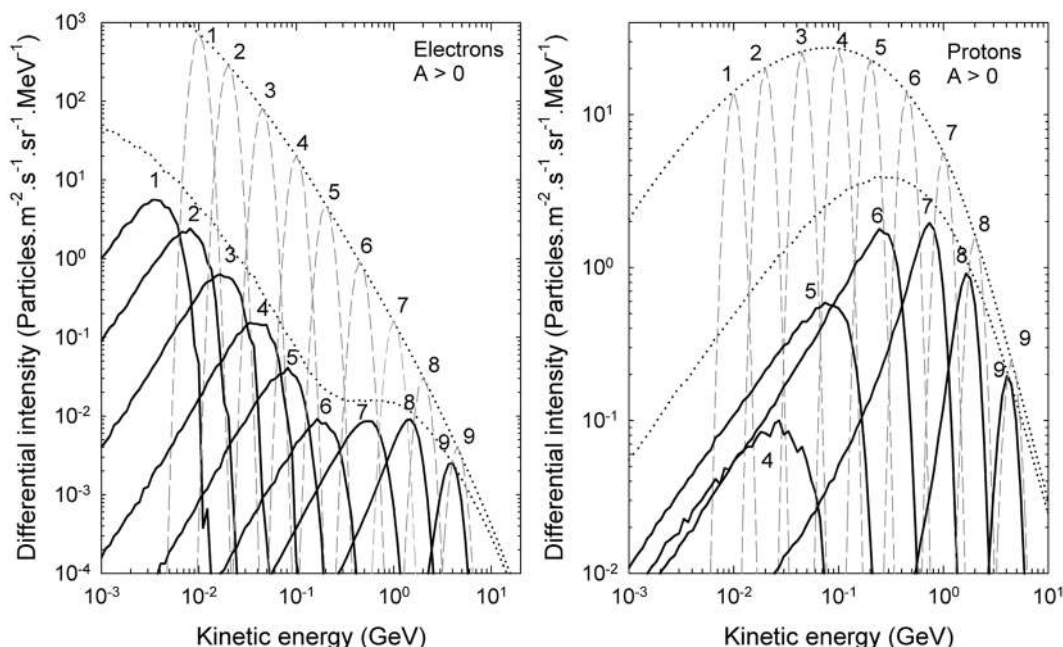


Figure 9. Modeled energy spectra at Earth for (left) electrons and (right) protons for the $A < 0$ HMF cycle using the 3D SDE model to illustrate the total effect of adiabatic energy losses under these drift conditions. Instead of a continuous function for the LIS, Gaussian peaks are specified at different energies (dashed grey lines), while the resulting spectra at Earth (for each of the numbered peaks independently) are shown as the solid lines. The dotted lines are the corresponding LIS and modulated solutions from Figure 8.

all of the peaks have a long “tail” distribution to lower energies. Characteristic of adiabatic cooling, proton spectra at Earth follow a $j \propto E$ spectrum at low energies, while electrons follow a $j \propto E^2$ trend [see, e.g., *Moraal and Potgieter, 1982*]. To calculate the “true” energy loss, the energy density of both the peaks and their counterparts at Earth, has to be integrated and the total energy density calculated. As demonstrated in the previous sections, the SDE approach does not have this limitation because the energy losses can be calculated directly for each pseudo-particle.

[39] A good test for the calculated τ and ΔE is illustrated in Figure 10. Above 1 GV, all transport coefficients for protons and electrons (as used in this study) are assumed to be exactly the same. The propagation times and rigidity loss of protons and electrons (in opposite drift cycles for the oppositely charged CRs) above 1 GV should thus be identical; a fact illustrated in Figure 10. The figure shows the rigidity loss (keeping in mind that the rigidity loss rate is independent of Γ) as a function of the propagation time at 5 GV and 10 GV and different drift cycles. We can thus summarize that protons and electrons at the same rigidity, will loose the same amount of rigidity adiabatically and have identical propagation times, if they had identical transport (drift and diffusion) coefficients.

[40] The modeled energy losses and propagation times of protons (Figure 11, top) and electrons (Figure 11, bottom) are shown as a function of energy (E^0) for both the $A > 0$ (Figure 11, left) and $A < 0$ (Figure 11, right) HMF polarity cycles. In contrast to the results of the previous sections, the 3D scenario is much more complex because of the addition of an energy dependent diffusion tensor and CR drifts.

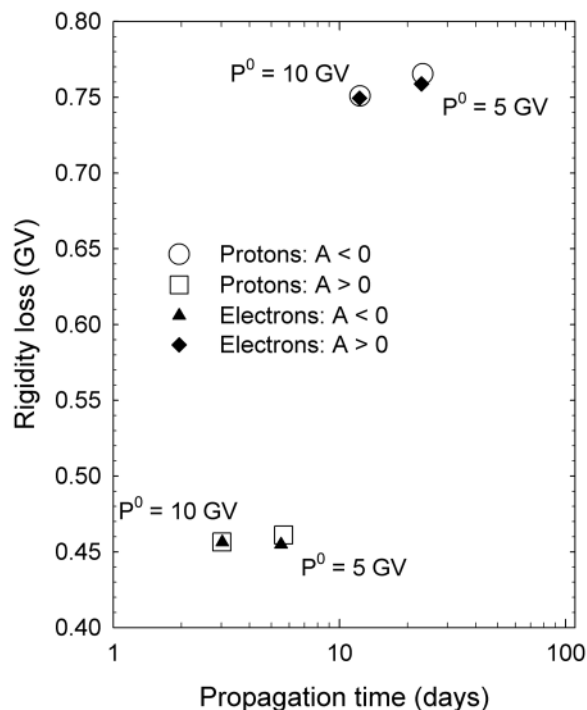


Figure 10. The rigidity loss of CR electrons and protons, plotted as a function of propagation time for $P^0 = 5$ GV and 10 GV and the two polarity cycles.

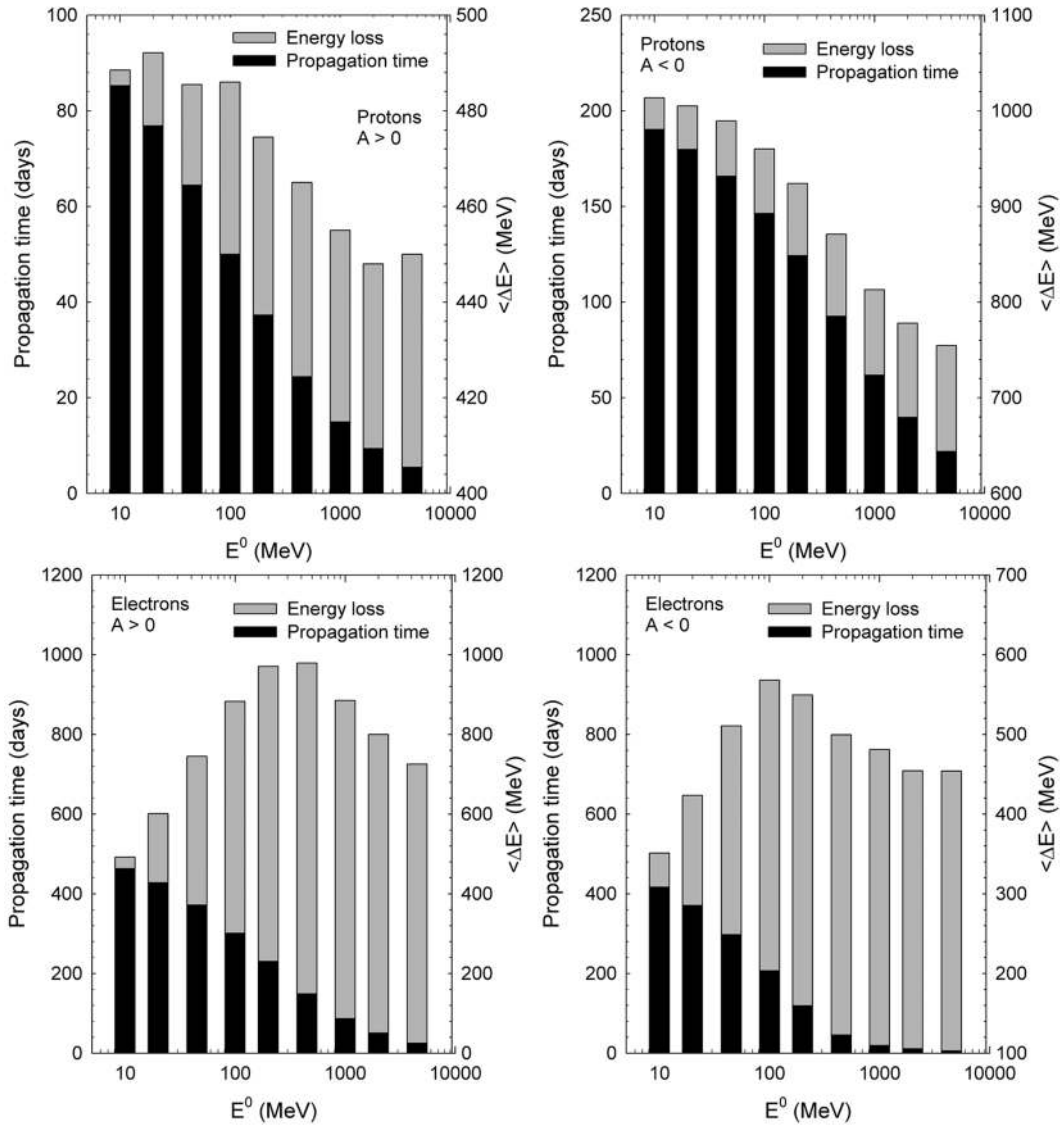


Figure 11. Calculated propagation times $\langle \tau \rangle$ and energy losses $\langle \Delta E \rangle$ of (top) protons and (bottom) electrons are shown for the (left) $A > 0$ and (right) $A < 0$ HMF polarity cycles. The propagation times are shown as black fills, while energy losses are indicated by grey fills.

Focussing first on protons, we note that for both drift cases the propagation time decreases with increasing energy, as expected because both the diffusion tensor and drifts increase with energy (rigidity). The propagation time is also much larger in the $A < 0$ than the $A > 0$ cycle. This is consistent with general drift considerations: For the $A < 0$ cycle, the protons that reach Earth have to drift inward along the heliospheric current sheet (HCS), taking a much longer time to reach Earth than protons which simply drift toward Earth from the polar regions in the $A > 0$ cycle. The energy losses suffered by the protons also decrease with increasing energy and is also larger for the $A < 0$ drift scenario. For electrons, the propagation times are qualitatively similar to those of the protons. The propagation time, $\langle \tau \rangle$, decreases with energy and is large for the $A > 0$ case (i.e., the drift cycle when electrons drift inward along the HCS). More intriguing is the fact that τ is much larger for electrons than protons at the same energy. For protons and electrons at the same energy,

the rigidity of the protons is much higher, and as the transport coefficients are expressed in terms of rigidity, the protons will have a much larger mean free path and drift speed and thus propagate faster than the electrons. The energy losses of electrons peak at intermediate energies, and decrease at high and low energies. This decrease at low energies (being absent for the proton case) is due to the electron diffusion coefficients being energy independent below $E \approx 1$ GeV. Electrons at, e.g., 10 MeV and 100 MeV will thus have the same diffusion coefficient, but the 100 MeV particles will lose more energy as the energy loss rate is proportional to E . More noteworthy is that the energy losses of electrons (at least at 100 MeV) are comparable to those of the protons. This is in contrast to the widely believed paradigm that electrons lose relatively little energy adiabatically [e.g., *Langner and Potgieter, 2004; Nkosi et al., 2008*]. This paradigm is based on the absence of the adiabatic limit $j \propto E^2$ in electron spectra observed

and modeled at Earth. As however discussed by *Moraal and Potgieter* [1982], this limit will only be seen when the net CR streaming is negligible; something that is more difficult to satisfy for electrons than protons. It might seem contradictory that electrons have longer propagation times than protons, yet loose equivalent amounts of energy adiabatically. One must however keep in mind that the energy loss rate is also proportional to Γ (see equation (24)), and that Γ is always larger for protons (for the energies considered here) than for electrons (see also Figure 7, right). This again illustrates the difficulty in calculating and interpreting the energy losses suffered by CRs.

6. Summary and Conclusions

[41] The propagation times and energy losses of CRs in the supersonic solar wind were calculated by making use of a SDE numerical modulation model with increasing complexity.

[42] First, the propagation times τ of CRs were calculated, for a spatially 1D scenario, with and without solar wind convection included in the model. These results were then compared successfully to analytical approximations, vindicating the SDE approach. The results indicate that τ is highly dependent on κ , as expected, and is generally longer when solar wind convection is included in the model as CRs find it more difficult to penetrate to the inner heliosphere. For the aforementioned scenario, the analytical approximations of *O'Gallagher* [1975] seem to be insufficient to describe τ . The reason for this is that he used the approximation $\kappa \ll 1$, a non-physical assumption because at these very small values of κ , convection dominates the diffusive process and CRs are unable to enter the heliosphere. The fractional energy loss of CRs was calculated, for the spatially 1D case and also compared successfully to analytical approximations. As with τ , we found that the energy loss increases with a decrease of κ . We also demonstrated that the energy loss of non-relativistic CRs is much larger than for relativistic particles due to the dependence on Γ (equation (24)) of the energy loss rate.

[43] With the SDE model thoroughly benchmarked, τ and ΔE (the average energy loss) were calculated for CR electrons and protons, for a spatially 3D scenario. The calculated values depend again strongly on the assumed transport (diffusion and drift) coefficients, with our choices of these parameters leading to τ decreasing with increasing energy. The drift cycle dependence of τ was also illustrated, with CRs having longer propagation times in the HMF cycle when they drift inward along the HCS toward Earth. We found that τ is much larger for electrons than protons at the same energy, as the electrons have a smaller mean free path (above rigidities of 1 GV for our choice of the diffusion tensor). The energy loss ΔE for protons also decreases with increasing energy and is largest in the $A < 0$ drift cycle. Due to the assumed energy independence of \mathbf{K} for electrons in this energy range, we found however that ΔE decreases at low energies. Moreover, we find ΔE for electrons to be smaller than for protons with the same energy, but larger than previously thought.

[44] In contrast to previous studies [e.g., *Gervasi et al.*, 1999], we are careful not to state that $\Delta E \propto \tau$. Referring back to equation (24), this will only be the case when the

energy loss rate (in the solar wind frame) is constant. The energy loss rate is however dependent on Γ , which is energy dependent, as well as E itself, making the process per definition non-linear. Moreover, it is also dependent on the quantity $\nabla \cdot \vec{V}_{sw}$. In this work we focused on the supersonic solar wind inside the TS, where $\nabla \cdot \vec{V}_{sw} > 0$ and adiabatic cooling consequently occurs. In the heliosheath however, a mixture of $\nabla \cdot \vec{V}_{sw} > 0$, $\nabla \cdot \vec{V}_{sw} = 0$, and $\nabla \cdot \vec{V}_{sw} < 0$ can occur. When $\nabla \cdot \vec{V}_{sw} < 0$, adiabatic heating of CRs can take place [e.g., *Langner et al.*, 2006] and equation (24) changes to an energy gain rate. When $\nabla \cdot \vec{V}_{sw} = 0$, no adiabatic energy changes can occur, even in the limit when $\tau \rightarrow \infty$.

[45] For future study, refinements to the present SDE model will be made in order to examine the effects of inserting a wavy current sheet and calculating, e.g., $\langle \tau \rangle$ as a function of solar activity, as well as the addition of a more realistic heliospheric geometry, i.e., to also include the effect of the heliosheath on the present results. Energy losses, on average, will be relatively small in the heliosheath, since $\nabla \cdot \vec{V}_{sw} \approx 0$. CR re-acceleration at the solar wind termination shock still needs to be investigated with the present model. This too would however not be significant for galactic cosmic rays as the Voyager spacecraft observed a much weaker than expected shock, with a compression ratio of only ~ 2 . In conclusion, comparing the energy losses that CRs experience inside the heliosphere as calculated with a SDE model, which includes CR drifts, with previous modeling results [e.g., *Potgieter and Moraal*, 1985] we find remarkable good agreement for both HMF polarity cycles. In addition, the SDE approach offers an exact method for calculating energy losses, directly from the numerical scheme, in a full 3D heliosphere, for which no analytical solutions are possible. The same applies to the calculation of the CR propagation times with the SDE approach. Comparing with ADI-based modulation models, the SDE approach gives significant additional insights into the modulation process, in particular into a subtle process such as adiabatic energy losses as described above.

[46] **Acknowledgments.** Philippa Browning thanks the reviewers for their assistance in evaluating this paper.

References

- Fichtner, H., J. A. le Roux, U. Mall, and D. Rucinski (1996), On the transport of pick-up ions in the heliosphere, *Astron. Astrophys.*, *314*, 650–662.
- Fisk, L. A. (1979), The interactions of energetic particles with the solar wind, in *Solar System Plasma Physics*, edited by E. N. Parker, C. F. Kennel, and L. J. Lanzerotti, pp. 177–227, North-Holland, Amsterdam.
- Florinski, V., and N. V. Pogorelov (2009), Four-dimensional transport of galactic cosmic rays in the outer heliosphere and heliosheath, *Astrophys. J.*, *701*, 642–651, doi:10.1088/0004-637X/701/1/642.
- Forman, M. (1970), The Compton-Getting effect for cosmic-ray particles and photons and the Lorentz-invariance of distribution functions, *Planet. Space Sci.*, *18*, 25–31, doi:10.1016/0032-0633(70)90064-4.
- Gardiner, C. W. (1983), *Handbook of Stochastic Methods*, Springer, Berlin.
- Gervasi, M., P. G. Rancoita, I. G. Usoskin, and G. A. Kovaltsov (1999), Monte-Carlo approach to galactic cosmic ray propagation in the heliosphere, *Nucl. Phys. B*, *78*, 26–31, doi:10.1016/S0920-5632(99)00518-6.
- Giacalone, J., and J. R. Jokipii (1999), The transport of cosmic rays across a turbulent magnetic field, *Astrophys. J.*, *520*, 204–214, doi:10.1086/307452.
- Gleeson, L. J., and W. I. Axford (1968), The Compton-Getting effect, *Astrophys. Space Sci.*, *2*, 431–437, doi:10.1007/BF02175919.
- Gleeson, L. J., and I. D. Palmer (1971), On the direct observation of cosmic-ray energy losses, *Astrophys. Space Sci.*, *12*, 137–146, doi:10.1007/BF00656143.

- Goldstein, M. L., L. A. Fisk, and R. Ramaty (1970), Energy loss of cosmic rays in the interplanetary medium, *Phys. Rev. Lett.*, *25*, 832–835, doi:10.1103/PhysRevLett.25.832.
- Jokipii, J. R., and E. N. Parker (1967), Energy changes of cosmic rays in the solar system, *Planet. Space Sci.*, *15*, 1375–1386, doi:10.1016/0032-0633(67)90111-0.
- Jokipii, J. R., and E. N. Parker (1970), On the convection, diffusion, and adiabatic deceleration of cosmic rays in the solar wind, *Astrophys. J.*, *160*, 735–744, doi:10.1086/150465.
- Kane, R. P. (1981), Scale size of the cosmic ray modulating region, *Astrophys. J.*, *246*, 1010–1013, doi:10.1086/158996.
- Kloeden, P. E., and E. Platen (1999), *Numerical Solution of Stochastic Differential Equations*, Springer, Berlin.
- Langner, U., and M. S. Potgieter (2004), Effects of the solar wind termination shock and heliosheath on the heliospheric modulation of galactic and anomalous helium, *Ann. Geophys.*, *22*, 3063–3072, doi:10.5194/angeo-22-3063-2004.
- Langner, U. W., O. C. de Jager, and M. S. Potgieter (2001), On the local interstellar spectrum for cosmic ray electrons, *Adv. Space Res.*, *27*, 517–522, doi:10.1016/S0273-1177(01)00100-4.
- Langner, U. W., M. S. Potgieter, H. Fichtner, and T. Borrmann (2006), Modulation of anomalous protons: Effects of different solar wind speed profiles in the heliosheath, *J. Geophys. Res.*, *111*, A01106, doi:10.1029/2005JA011066.
- Maruyama, G. (1955), Continuous Markov processes and stochastic equations, *Rend. Circolo Mat. Palermo*, *4*, 48–90.
- Moraal, H., and M. S. Potgieter (1982), Solutions of the spherically-symmetric cosmic-ray transport equation in interplanetary space, *Astrophys. Space Sci.*, *84*, 519–533, doi:10.1007/BF00651330.
- Moskalenko, I. V., A. W. Strong, J. F. Ormes, and M. S. Potgieter (2002), Secondary antiprotons and propagation of cosmic rays in the galaxy and heliosphere, *Astrophys. J.*, *565*, 280–296, doi:10.1086/324402.
- Nkosi, G. S., M. S. Potgieter, and S. E. S. Ferreira (2008), Electron anisotropies in the inner heliosphere, *Planet. Space Sci.*, *56*, 501–509, doi:10.1016/j.pss.2007.10.003.
- O’Gallagher, J. J. (1975), A time-dependent diffusion-convection model for the long-term modulation of cosmic rays, *Astrophys. J.*, *197*, 495–507, doi:10.1086/153535.
- Øksendal, B. (2003), *Stochastic Differential Equations: An Introduction With Applications*, Springer, Berlin.
- Parker, E. N. (1958), Dynamics of the interplanetary gas and magnetic fields, *Astrophys. J.*, *128*, 664–676, doi:10.1086/146579.
- Parker, E. N. (1965), The passage of energetic charged particles through interplanetary space, *Planet. Space Sci.*, *13*, 9–49, doi:10.1016/0032-0633(65)90131-5.
- Parker, E. N. (1966), The effect of adiabatic deceleration on the cosmic ray spectrum in the solar system, *Planet. Space Sci.*, *14*, 371–380, doi:10.1016/0032-0633(66)90074-2.
- Pei, C., J. Bieber, R. A. Burger, and J. Clem (2010), A general time-dependent stochastic method for solving Parkers transport equation in spherical coordinates, *J. Geophys. Res.*, *115*, A12107, doi:10.1029/2010JA015721.
- Potgieter, M. S., and H. Moraal (1985), A drift model for the modulation of galactic cosmic rays, *Astrophys. J.*, *294*, 425–440, doi:10.1086/163309.
- Strauss, R. D., M. S. Potgieter, I. Büsching, and A. Kopp (2011), Modeling the modulation of galactic and Jovian electrons by stochastic processes, *Astrophys. J.*, *735*, 83–96, doi:10.1088/0004-637X/735/2/83.
- Urch, I. H., and L. J. Gleeson (1973), Energy losses of galactic cosmic rays in the interplanetary medium, *Astrophys. Space Sci.*, *20*, 177–185, doi:10.1007/BF00645595.
- Webb, G. M., and L. J. Gleeson (1979), On the equation of transport for cosmic-ray particles in the interplanetary region, *Astrophys. Space Sci.*, *60*, 335–351, doi:10.1007/BF00644337.
- Webb, G. M., and L. J. Gleeson (1980), Cosmic-ray flow lines and energy changes, *Astrophys. Space Sci.*, *70*, 3–31, doi:10.1007/BF00641662.
- Yamada, Y., S. Yanagita, and T. Yoshida (1998), A stochastic view of the solar modulation phenomena of cosmic rays, *Geophys. Res. Lett.*, *25*, 2353–2356, doi:10.1029/98GL51869.
- Zhang, M. (1999), A Markov stochastic process theory of cosmic-ray modulation, *Astrophys. J.*, *513*, 409–420, doi:10.1086/306857.

I. Büsching, Institut für Theoretische Physik, Ruhr-Universität Bochum, D-44780 Bochum, Germany. (ib@tp4.rub.de)

A. Kopp, Institut für Experimentelle und Angewandte Physik, Christian-Albrechts-Universität zu Kiel, Leibnizstraße 11, D-24118 Kiel, Germany. (kopp@physik.uni-kiel.de)

M. S. Potgieter and R. D. Strauss, Centre for Space Research, North-West University, 10 Hoffman St., Potchefstroom 2522, South Africa. (marius.potgieter@nwu.ac.za; dutoit.strauss@nwu.ac.za)